INTERNATIONAL JOURNAL FOR NUMERICAL METHODS IN FLUIDS
Int. J. Numer. Meth. Fluids 2009; **61**:453–472
Published online 21 November 2008 in Wiley InterScience (www.interscience.wiley.com). DOI: 10.1002/fld.1966

Numerical studies of blood flow in healthy, stenosed, and stented carotid arteries

Mickaël Gay and Lucy T. Zhang*, †

Department of Mechanical, Aerospace, and Nuclear Engineering, Rensselaer Polytechnic Institute, Troy, NY 12180, U.S.A.

SUMMARY

Numerical analysis of pulsatile blood flow in healthy, stenosed, and stented carotid arteries is performed with the aim of identifying hemodynamic factors in the initiation, growth, and the potential of leading to severe occlusions of a diseased artery. The Immersed Finite Element Method is adopted for this study to conveniently incorporate various geometrical shapes of arteries without remeshing. Our computational results provide detailed quantitative analysis on the blood flow pattern, wall shear stress, particle residence time, and oscillatory shear index. The analysis of these parameters leads to a better understanding of blood clot formation and its localization in a stenosed and a stented carotid artery. A healthy artery is also studied to establish a baseline comparison. This analysis will assist in developing treatments for diseased arteries and novel stent designs to reduce restenosis. Copyright © 2008 John Wiley & Sons, Ltd.

Received 16 October 2007; Revised 2 June 2008; Accepted 10 October 2008

KEY WORDS: carotid artery; stenosis; stent; wall shear stress; oscillatory shear index; residence time; Immersed Finite Element Method

1. INTRODUCTION

Currently, stroke is the third leading cause of death in the United States [1] with more than 700 000 Americans experiencing a stroke each year. Stenoses and occlusions of carotid arteries are involved in 34–44% of strokes [2, 3]. The development of a gradual stenosis in the arteries limits oxygen transport to tissues and dependent organs. It is believed that thrombi formed within and distal to the stenoses pose clinical threats. In the case of carotid arteries, the clinical threat is largely due

*Correspondence to: Lucy T. Zhang, Department of Mechanical, Aerospace, and Nuclear Engineering, Rensselaer Polytechnic Institute, Troy, NY 12180, U.S.A.
†E-mail: zhangLucy@rpi.edu

to the embolization arising from an atherosclerotic plaque or acute occlusion of the artery and the downstream propagation of the thrombus [4].

Platelets play a vital role in initiating thrombosis within stenosed arteries. The mechanical force most relevant to platelet-mediated hemostasis and thrombosis is wall shear stress, a quantity not easily measurable *in vivo*. The relationship between flow in arteries, particularly the wall shear stress, and the sites where atherosclerosis develops has motivated much of the research in arterial flow in recent decades [5–10]. Shear-induced platelet activation and aggregation depend on several factors that include (1) level of shear stress, (2) spatial variation in shear stress, and (3) temporal variation in shear stress. It has been proposed that very high shear conditions ($>15\,\mathrm{dyn/cm^2}$) may initiate thrombosis [11], leading to thromboembolic strokes [12–14]. Several theoretical studies have been done to predict the location of maximum wall shear stress in a stenosed artery [5–10, 15, 16]. Among these studies, Ku *et al.* [17] and Wootton and Ku [18] pointed out that the highest wall shear stress often occurs at the throat of a stenosis. On the other hand, it has been well accepted that blood is clotted by a cascade of coagulation proteins when it is exposed to very low shear stress [17, 19–21] or when it changes rapidly in time (factor 2) or space (factor 3) [17, 22]. Most intimal thickening occurs where the average wall shear stress is less than $10\,\mathrm{dyn/cm^2}$ [9, 11, 23]. These conditions are likely to prevail at places where the vessel is curved, bifurcates, has a junction, a side branch, or other sudden change in flow geometry [24, 25], and when the flow is unsteady [17, 26]. The severe stenosis may also cause changes in the mechanical properties of the surrounding walls [27–32]. Various *in vitro* studies [33–35] have shown that regions of increased blood residence time promote fibrin thrombus formation. As a result of prolonged residence time, the platelet-rich thrombus that forms at the stenosis apex extends downstream and forms a stagnation thrombus [36–38]. The danger of a stagnation thrombus is that it may grow to several centimeters in length [38] and completely fill the stagnant flow region [35, 39]. It may eventually embolize, propagate down the arterial tree, and become lodged in a small artery or a side branch.

To reduce or remove the obstructions that block a normal blood flow, angioplasty and stents were introduced to dilate the area of arterial blockage. Despite their success and widespread use, outcomes for patients receiving stents are still hampered by thrombosis and restenosis, which occur in 20–30% of the cases following the prostheses implantation [40]. A number of medical and computational studies [41–46] suggest that relatively small disturbances in the flow such as the struts of a stent may result in significant changes in the wall shear stress.

Considering the strong correlations between the arterial wall shear stress, particle residence time, and localization of thrombus formation, quantifying these hemodynamic parameters is important in understanding the development of arterial diseases, specifically how a thrombus is initiated and promoted. Thus, the goal of this study is to adopt a feasible computational technique that can quantify these hemodynamic factors using three types of carotid arteries: healthy, stenosed, and stented. The objectives of this study are threefold: (1) to quantify and assess hemodynamic factors associated with stenosis, (2) to evaluate the mutual effect between the progression of stenosis and stenosis-induced changes in local hemodynamic conditions, and (3) to evaluate at which degree the stent can potentially induce the development of restenosis. By evaluating regional hemodynamic changes for healthy, stenosed, and stented arteries, it is hoped that the development of diseases can be better explained through the view of fluid dynamics, which may ultimately result in better prevention and treatment techniques.

In this paper, we first review the numerical algorithm, the Immersed Finite Element Method (IFEM) [47, 48], used for this study with enhanced interface treatment for rigid embedded structures

DOI: 10.1002/fld

in Section 2. In Sections 3–5, we present the modeling and analysis of two-dimensional unsteady pulsatile flows in a healthy carotid artery and in stenosed and stented arteries that are most relevant in the context of thrombus formation. Finally, conclusions and remarks are presented in Section 6.

2. SIMULATION TECHNIQUE AND HEMODYNAMIC QUANTITIES

2.1. Immersed Finite Element Method

In this study, we will adopt the IFEM [47, 48] that was recently developed to solve complex fluid and deformable structure interaction problems. It has been successfully used to model various biomechanics applications including shear-induced red blood cell deformation [49], stent deployment [50], and flow in cardiovascular systems [51]. This numerical technique provides the flexibilities in handling varying shapes of embedded structures. Therefore, it can be conveniently adopted in this study where the immersed structures, i.e. stenosed and stented arteries, come in different shapes and geometries. The diameter change of a carotid artery during a cardiac cycle is observed to be minimal, approximately 5–10% with a high degree of stiffness. Therefore, rigid artery walls are assumed in this study. However, if different material properties are to be considered for stenotic arteries, this numerical technique can be easily used to accommodate the deformability in stenotic arteries and their corresponding influences in the fluid flow.

In the IFEM algorithm, two sets of domains are considered: a solid structure with Lagrangian description and an incompressible fluid domain (or background grid) with Eulerian description. This setup allows us to generate fluid and solid meshes and solve fluid and solid equations independently, thus avoiding frequent mesh updating schemes. The embedded solid can move freely within the fluid domain. The interactions between the fluid and the solid are computed through interpolations of velocities and forces at the fluid–structure interface.

The no-slip boundary condition at the interface ensures the solid velocity at the solid boundary to be equal to the surrounding fluid velocity. When dealing with a rigid structure the interaction force acting on the solid structure $\mathbf{f}^{\mathrm{FSI,s}}$ can be calculated using the opposing force that is induced by the surrounding fluid such that

$$\mathbf{f}^{\mathrm{FSI,s}} = \rho\left(\frac{\partial \mathbf{v}^{\mathrm{s}}}{\partial t} + \mathbf{v}^{\mathrm{s}} \cdot \nabla \mathbf{v}^{\mathrm{s}}\right) + \nabla p^{\mathrm{s}} - \mu \nabla^2 \mathbf{v}^{\mathrm{s}} \tag{1}$$

where $\mathbf{v}^{\mathrm{s}}$ and p^{s} are the solid velocity and pressure on a solid boundary node $\mathbf{X}^{\mathrm{s}}$, which are interpolated from the known surrounding fluid velocities and pressure. Details of the interpolation process are given in [52]. It must be noted that this force is evaluated only at the interface since there is no internal force generated inside a rigid solid.

The interaction force $\mathbf{f}^{\mathrm{FSI,s}}(\mathbf{X}^{\mathrm{s}}, t)$ is then distributed onto the nodes in the fluid domain $\mathbf{f}^{\mathrm{FSI}}(\mathbf{x}, t)$ using an interpolation function that was used as the shape function in one of the meshfree methods called Reproducing Kernel Particle Method [53, 54]:

$$\mathbf{f}^{\mathrm{FSI}}(\mathbf{x}, t) = \int_{\Omega} \mathbf{f}^{\mathrm{FSI,s}}\, \Phi(\mathbf{x} - \mathbf{x}^{\mathrm{s}})\, \mathrm{d}\Omega \tag{2}$$

where $\Phi(\mathbf{x} - \mathbf{x}^{\mathrm{s}})$ is the interpolation function that is defined as a function of the distance between a solid node at position $\mathbf{x}^{\mathrm{s}}$ and its surrounding fluid nodes at $\mathbf{x}$. Once distributed onto the fluid

DOI: 10.1002/fld

domain, this interaction force serves as an external force in the fluid domain. Fluid velocities $\mathbf{v}$ and pressure p are then solved iteratively from the Navier–Stokes equations:

$$\rho^{\mathrm{f}}(\mathbf{v}_{,t}+\mathbf{v}\cdot\nabla\mathbf{v})=-\nabla p+\mu\nabla^2\mathbf{v}+\mathbf{f}^{\mathrm{FSI}} \tag{3}$$

$$\nabla\cdot\mathbf{v}=0 \tag{4}$$

These equations are solved repeatedly for every time step with a semi-explicit time integration scheme. The accuracy of this method has been extensively studied in [52].

2.2. *Fluid quantities in arterial flow*

Three important hemodynamic quantities will be examined in this study: (1) wall shear stress, (2) oscillation shear index (OSI) that measures the direction of the wall shear stress, and (3) particle residence time that measures the average time that a particle (platelet) remains in a region.

The wall shear stress, τ_{w}, is computed from the instantaneous velocity vector field $\mathbf{v}$ as follows:

$$\tau_{\mathrm{w}}=-\mu\frac{\partial\mathbf{v}}{\partial r} \tag{5}$$

where r is the distance from the wall in the transverse direction of the flow. In numerical simulations, the wall shear stress is measured at a layer near the wall inside the channel (at around 0.01 mm apart from the wall).

The OSI is formulated to account for the cyclic departure of the wall shear stress vector from its predominant axial alignment. It is calculated on the basis of its standard definition [20] as

$$\mathrm{OSI}=\frac{1}{2}\left(1-\frac{|\int_0^T\tau_{\mathrm{w}}\,\mathrm{d}t|}{\int_0^T|\tau_{\mathrm{w}}|\,\mathrm{d}t}\right) \tag{6}$$

where T is the duration of the cycle and τ_{w} is the instantaneous shear stress. This index represents a measure of the shear stress acting on the luminal surface due to either cross flow or reverse flow that occurs in a pulsatile flow. It describes the degree of deviation of the wall shear stress from its average direction. This index may not describe the pattern (e.g. frequency, intermittence) of oscillation, but rather shows the significance of oscillations in a flow. The maximum OSI can reach 0.5. In the regions where OSI value is near 0.5, the wall is subjected to high oscillating shear stresses. In regions of unidirectional flow, OSI reaches zero.

A characteristic dimensionless residence time, T_{r}, of a fluid particle in the vicinity of an irregular surface is correlated with the wall shear stress and can be estimated according to Himburg *et al.* [55] as

$$T_{\mathrm{r}}\sim\frac{\mu}{T}[(1-2\,\mathrm{OSI})\langle\tau_{\mathrm{w}}\rangle]^{-1} \tag{7}$$

where $\langle\cdot\rangle$ represents the time-averaged quantity. In this definition, OSI acts to include the effect of time-averaged shear stress on the residence time at a site. When the OSI is small, it has little effect on the residence time, but as it approaches its limit of 0.5, it can have an increasingly important influence on this quantity. Using the techniques presented above, it is possible to evaluate precisely where and how long particles will reside within a given configuration.

DOI: 10.1002/fld

3. HEALTHY ARTERY

We first consider a straight two-dimensional artery with two walls separated by a distance of $d=0.5\,\text{cm}$. The artery walls are $L=5.0\,\text{cm}$ long and $t=0.07\,\text{cm}$ thick embedded in a fluid domain of length $L=5.0\,\text{cm}$ and width $D=0.8\,\text{cm}$ as shown in Figure 1. A thinner mesh is used near the walls to ensure accuracy at the interfaces.

Pulsatile flow is considered, where the inflow velocity is based on a time-dependent flow rate Q obtained from the experiments of Holdsworth *et al.* [56] as shown in Figure 1. The waveform has a period $T=0.9\,\text{s}$ (67 beats per minute), where $0\,\text{s}<t<0.4\,\text{s}$ is systolic and $0.4\,\text{s}<t<0.9\,\text{s}$ is diastolic. The maximum systolic velocity is 117.35 cm/s and the time-averaged velocity is 30.69 cm/s. Blood is considered to be homogeneous and incompressible with a constant density $\rho^{\text{f}}=1.055\,\text{g/cm}^3$ and viscosity $\mu=0.035\,\text{dyn s/cm}^2$. The maximum Reynolds number, given by $Re_{(\max)}=\rho\,\text{d}u_{\max}/\mu$, is 1769 and the inlet pulse has a mean Reynolds number of 463. A critical parameter in this analysis is the Womersley number, defined as $\alpha=r(\omega/v)^{1/2}$, where ω is the angular frequency of the driving pulse, r is the radius of the vessel, and v is the kinematic viscosity of the blood. For this given blood flow, a Womersley number of 3.63 is observed. A summary of the parameters is given in Table I. These parameters are also in agreement with physiologic observations, which for a medium-sized artery have a Reynolds number of typically on the order of 100–1000 and a Womersley parameter that ranges from 1 to 10 [57].

The results reported in this paper are obtained during the third time period, i.e. $1.8\,\text{s}<t<2.7\,\text{s}$, when the flow has reached a stable periodic solution. Velocity profiles at six different time steps

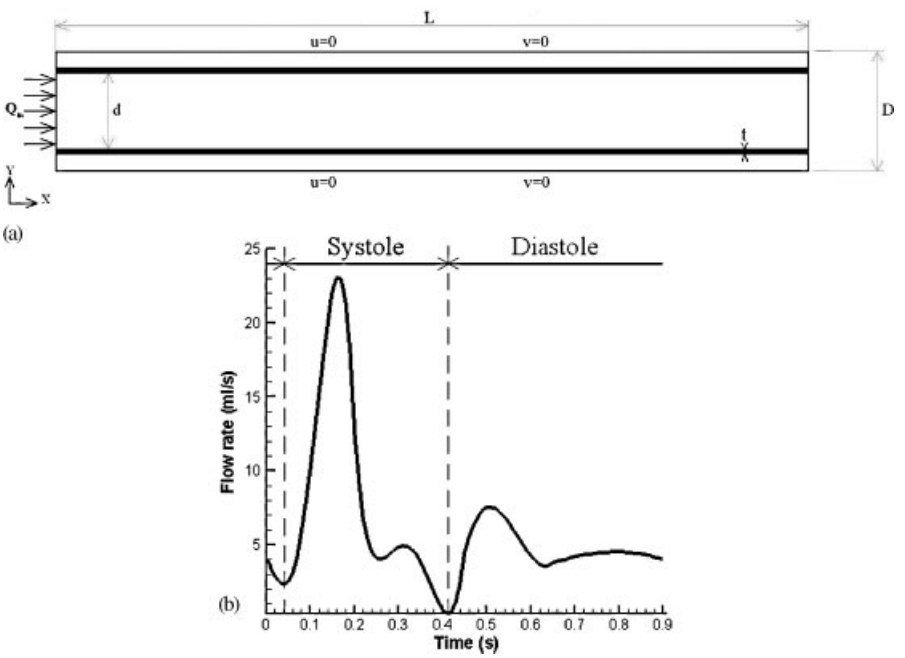

Figure 1. Pulsatile flow in a healthy carotid artery: (a) schematic of pulsatile flow in a healthy carotid artery and (b) flow rate from Holdsworth *et al.* [56].

DOI: 10.1002/fld

Table I. Carotid artery flow parameters.

Parameters	Value
Blood density: ρ^{f}	$1.055\,\mathrm{g/cm^3}$
Blood dynamic viscosity: μ^{f}	$0.035\,\mathrm{dyn\,s/cm^2}$
Blood pulse period: T	0.9 s
Artery diameter: d	0.5 cm
Artery length: L	5 cm
Artery thickness: t	0.07 cm
Maximum inflow velocity: $u_{\max}$	117.35 cm/s
Mean inflow velocity: $\bar{u}$	30.69 cm/s
Maximum Reynolds number: $Re_{(\max)}$	1769
Mean Reynolds number: $\bar{Re}$	463
Womersley number: α	3.63

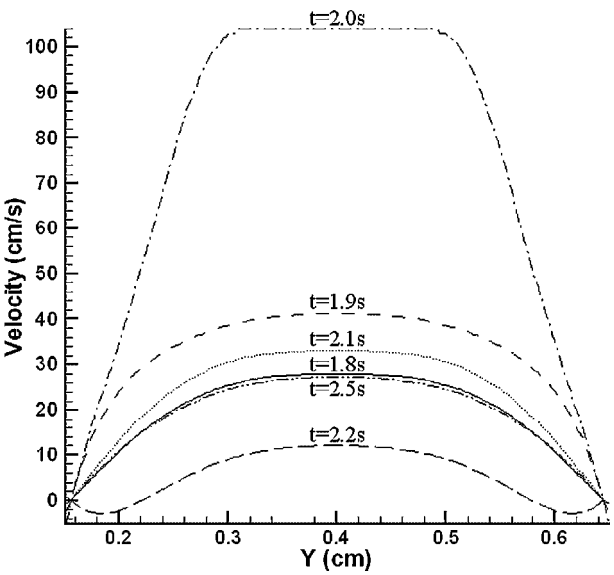

Figure 2. Velocity profiles in a straight rigid carotid artery during a cardiac cycle.

during the pulsation are shown in Figure 2. As expected for this Womersley number, the inertial force dominates. The velocity profiles turn into plug flow shapes and the centerline velocity oscillates with the driving pulse. At the end of systole ($t = 2.2$ s), blood flow changes direction near the boundary layer due to the effect of viscous forces. These forces influence the velocity profiles in a way that, when the pressure gradient reverses, the flow near the wall changes direction. This flow behavior is in agreement with the results presented by Berbich *et al.* [58].

Correspondingly, the wall shear stress varies and oscillates with the cardiac cycle because of the pulsatile changes in the velocity and direction of the blood flow. From our computational results, we obtain a mean-average wall shear stress (the temporal mean over the cardiac cycle and the spatial average along the wall) of $8.11\,\mathrm{dyn/cm^2}$ and a peak wall shear stress of $36.55\,\mathrm{dyn/cm^2}$.

DOI: 10.1002/fld

Table II. Summary of wall shear stress measurements in carotid arteries (units in dyn/cm^2).

Parameters	Peak wall shear stress	Mean-average wall shear stress
IFEM	36.55	8.11
Dammers *et al.* [59]	34.0 ± 8.0	11.5 ± 2.1
Samijo *et al.* [65]	33 ± 6.8	12 ± 1.8
Oshinski *et al.* [63]		8.0 ± 4.1
Gnasso *et al.* [60]	29.5 ± 8.2	12.1 ± 3.1
Gnasso *et al.* [61]	18.7 ± 4.1	15.3 ± 4.0
Hoeks *et al.* [62]	22.4	7.0
Oyre *et al.* [64]	25.6	9.5

We compared our results with a collective experimental measurement of mean-average and peak wall shear stresses gathered from References [59–65] in Table II. The computed mean-average and peak wall shear stresses are in good agreement with these previous experimental results.

4. STENOSED ARTERY

Stenosed (constricted) arteries with varying severities of stenosis under physiologic conditions are studied in this section. The computational model and properties are built based on the healthy artery detailed in Section 3. A symmetric constriction is imposed at the center of the artery far from the outlet so that the flow can return to a nearly fully developed state and the outlet boundary does not influence activities occurring upstream. In clinical medicine, the severity of stenoses is commonly defined as the percentage of occlusion using diameter measurements: % stenosis$=$ $(d_1-d_2)/d_1*100\%$, where d_1 is the artery diameter and d_2 is the constricted diameter. As the disease advances, the percentage of stenosis also increases. Two separate studies will be performed. We first consider a stenosed artery with a moderate 50% stenosis, as depicted in Figure 3, where detailed hemodynamic parameters will be analyzed. Second, we will examine the effects of the fluid quantities with varying severities of stenosis, from mild to severe (40–76%).

4.1. Analysis of a moderate stenosis (50%)

4.1.1. Velocity. The X-component of velocity contours at different instances over one cardiac cycle is shown in Figure 4. The constriction generates a fluid jet velocity profile during systole ($1.8\,\text{s}<t<2.2\,\text{s}$). In this jet region, the flow is accelerated with a high forward flow in the axial direction. During diastole ($2.2\,\text{s}<t<2.7\,\text{s}$) deceleration of fluid velocity and large recirculating zone is observed downstream of the stenosis. There is also a near stagnation zone at the foot of the stenosis and several eddies form downstream of the stenosis. Similar results were observed by Rosenfeld and Einav [66]. The velocity profiles at different locations along the channel are plotted in Figure 5. In the downstream of the stenosis ($X\geqslant2.65\,\text{cm}$), the flow decelerates and reverses near the wall, as they are most obviously observed in Figure 5(c–f). The presence of a constriction in the artery alters the pulsatile velocity waveforms by blocking higher frequencies and blunting the amplitude at the end of systole.

4.1.2. Shear stress. These complex changes in blood velocities can create significant changes in the wall shear stress. Figure 6 shows the wall shear stress during one cardiac cycle at different

DOI: 10.1002/fld

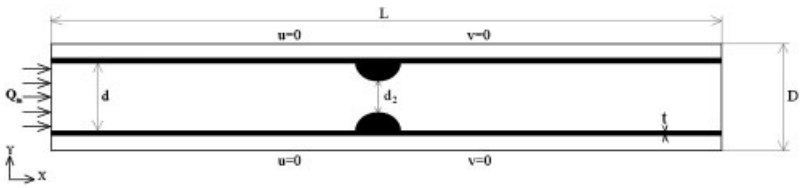

Figure 3. Pulsatile flow in a constricted carotid artery.

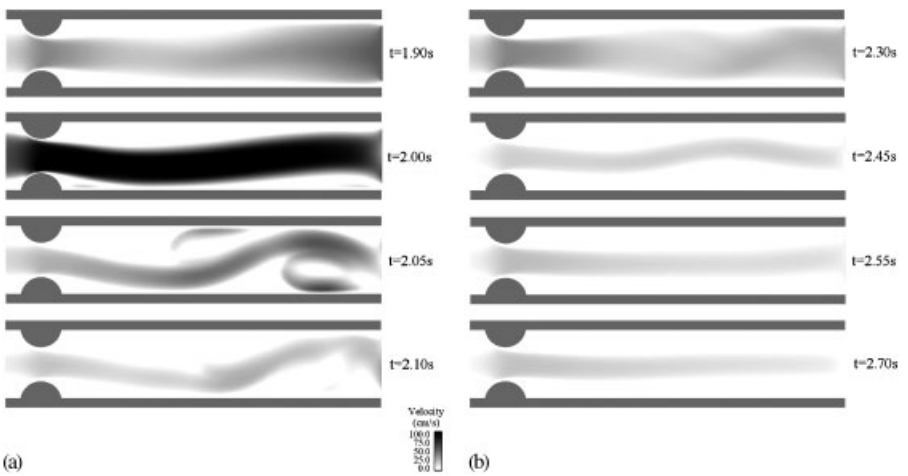

Figure 4. Velocity contours in a moderate (50%) stenosed artery during a cardiac cycle: (a) systole and (b) diastole.

locations around the constriction. The wall shear stress increases sharply at the upstream of the constriction (points 3–5). The peak value is identified at the tip of the constriction (point 5) at the end of systole. On the other side of the constriction and during diastole, low wall shear stress is observed (points 7 and 8). Around the constriction, we observe a maximum value of the wall shear stress $\tau_{\text{wall(peak)}}$ to be 388 dyn/cm^2 and a time-averaged value $\tau_{\text{wall(mean)}}$ of 93.8 dyn/cm^2 near the throat (at an angle of $\sim 78°$) (Figure 6), which are in the physiologic range as reported in [13, 67]. Studies from Holme *et al.* [68] and Sakariassen *et al.* [69] concluded that a shear stress threshold of 315 dyn/cm^2 is sufficient to induce significant platelet activation and micro-particle formation. Thus, our results suggest that the sudden spatial change (stenosis) increases the wall shear stress dramatically compared with a healthy artery where the shear stress is found to be 36.55 dyn/cm^2 from the previous study in Section 3. This high wall shear stress might be an important factor for activation and thrombus formation for a moderate stenosis.

4.1.3. Oscillatory shear index. In the downstream of the stenosis ($X > 2.65$ cm), the strong unsteady flow causes a corresponding unsteadiness in the wall shear stress field. The mean wall shear stress is found to be very low and oscillating between positive and negative values along the longitudinal direction as plotted in Figure 7. This oscillatory behavior of shear stress is best represented by

DOI: 10.1002/fld

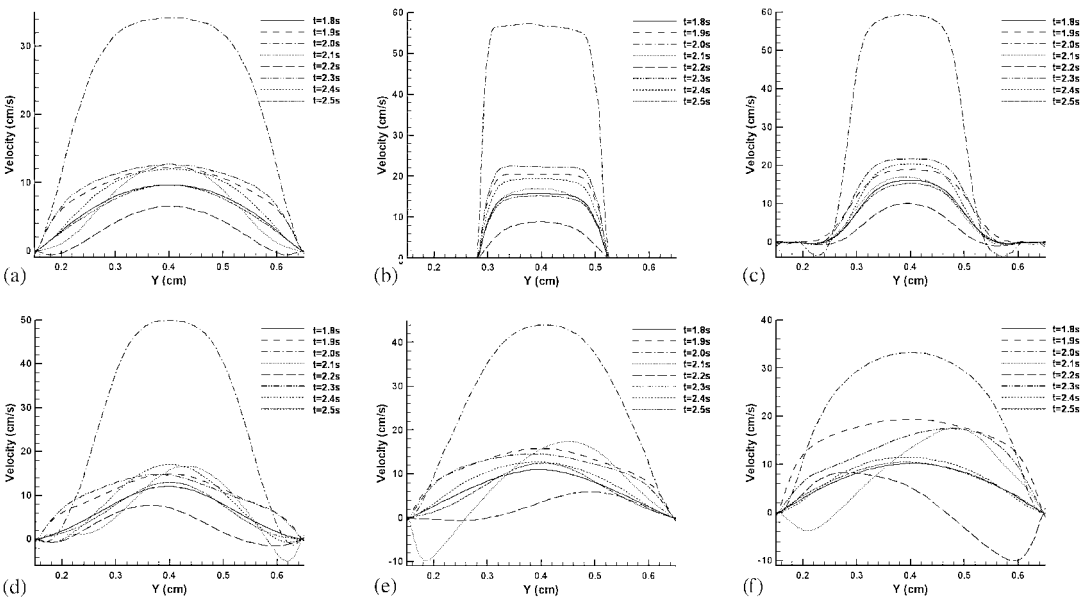

Figure 5. Velocity profiles at different locations in a moderate (50%) stenosis during a cardiac cycle: (a) $X=2.0\,\text{cm}$; (b) $X=2.5\,\text{cm}$; (c) $X=2.65\,\text{cm}$; (d) $X=3.5\,\text{cm}$; (e) $X=4.0\,\text{cm}$; and (f) $X=4.8\,\text{cm}$.

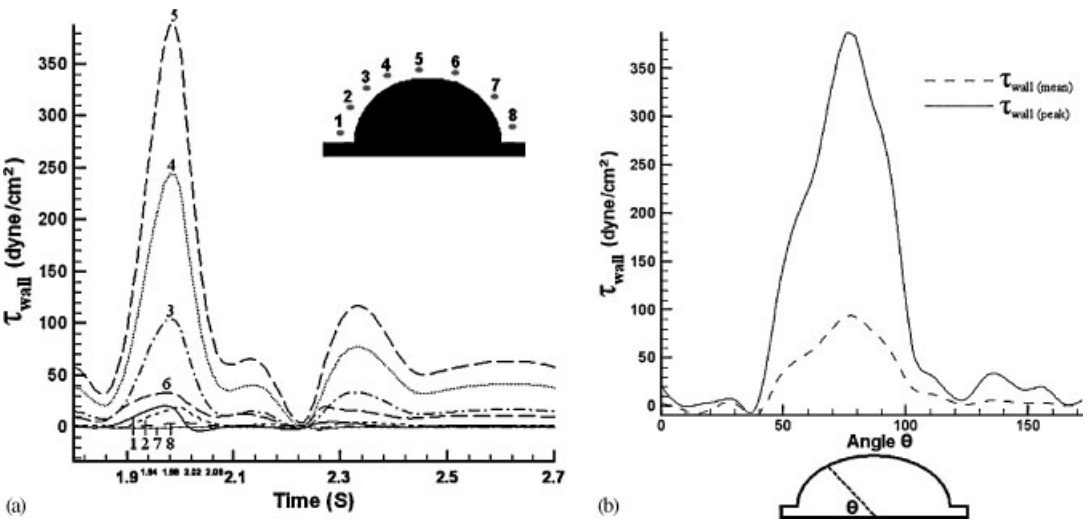

Figure 6. Wall shear stress at different locations around a moderate (50%) stenosis during one cardiac cycle: (a) wall shear stress during a cardiac cycle and (b) mean and peak wall shear stresses around a moderate (50%) constriction.

DOI: 10.1002/fld

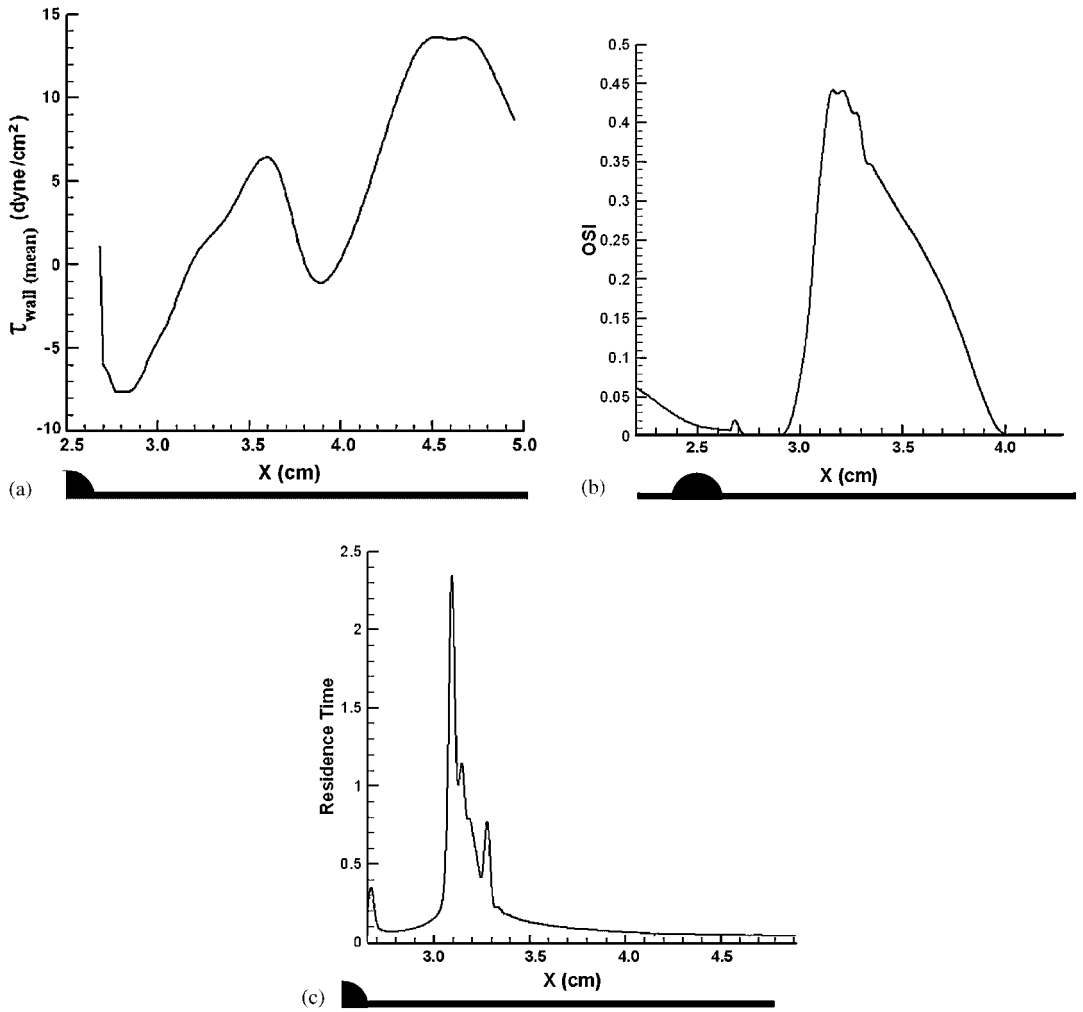

Figure 7. Arterial flow quantities (mean wall shear stress, oscillatory shear index, and residence time) at downstream of a moderate (50%) constriction: (a) mean wall shear stress; (b) oscillatory shear index; and (c) residence time.

a parametric study of the OSI. The OSI is examined at around the stenosis and downstream of the flow as shown in Figure 7. Around the stenosis a low and decreasing OSI is observed, while downstream a very high OSI appears with a maximum value of 0.44, which means that the wall is subjected to high oscillating shear stress or regions of flow reversal. By investigating the distribution patterns of mean wall shear stress and OSI in relation to the features of the intravascular flows, it is easy to find that the low mean wall shear stress and high OSI regions coincide well with the regions where flow separations are present. Longest and Kleinstreuer [70] suggested that regions exposed to a high OSI are more susceptible to plaque formation, which in our model would be downstream of the constriction.

DOI: 10.1002/fld

4.1.4. Residence time. The last hemodynamic parameter under investigation in the current study is the residence time. The probability of a given platelet triggering a thrombus formation depends on the residence time available for platelet activation and on the local wall shear stress. Since the region immediately downstream of an arterial stenosis induces an abrupt reduction in wall shear stress and low reversing velocities, local residence time may be an important factor in determining degrees of stenoses and types of flow conditions that might be most conducive to platelet adhesion. The computed residence time downstream of the stenosis is presented in Figure 7. During diastole, the deceleration and reversal of flow downstream of the stenosis with the presence of a weak forward jet and large recirculation zones lead to extended particle path lengths and greater residence times. With a high residence time, activated platelets may recirculate in the separated region long enough to form small aggregates. Our results agree with the simulation studies obtained from Kunov *et al.* [71] who quantified platelet residence times in the region of an axisymmetric 45% area reduction stenosis.

4.2. Analysis of varying degrees of stenosis (40–76%)

The severity of stenosis is an important determinant of the wall shear stresses, OSI, and particle residence time. We conduct our study for mild (40%), moderate (50, 60%), and severe (70, 76%) stenoses with a smooth symmetric plaque surface morphology.

4.2.1. Velocity. For all degrees of stenosis, a relatively large recirculation region is found to exist downstream of the constriction (Figure 8). This figure shows that increasing the size of a constricted region corresponds to increasing number of vortices with higher strength. These recirculation zones are indications of regions where the flow is reversed in a significant portion of each cycle.

4.2.2. Shear stress. The severity of the stenosis affects the shear stress characteristics significantly, especially at the tip of the stenosis. There is a very significant increase in shear stress with increasing level of severity of stenosis. We found that for the most severely stenosed case, the magnitude

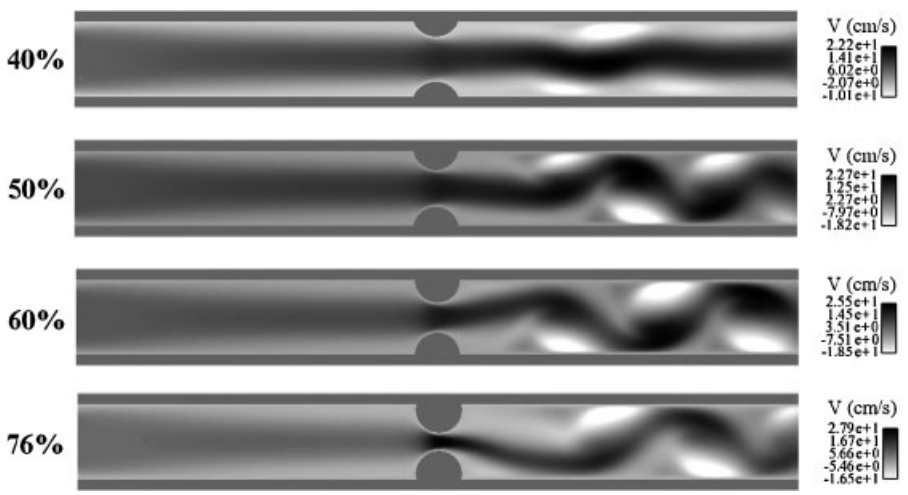

Figure 8. Velocity contours of flows in varying degrees of stenosis.

DOI: 10.1002/fld

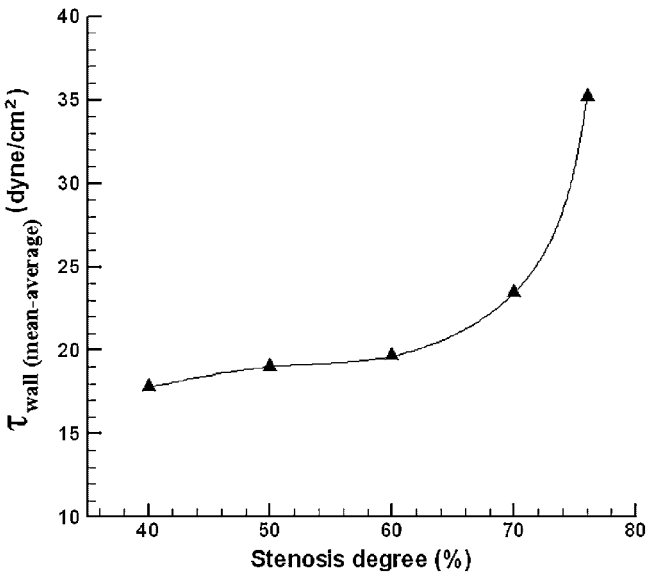

Figure 9. Mean-average wall shear stress of the constriction as a function of degree of stenosis.

of the peak value reaches more than 14 times of the unstenosed case found in Section 3, similar to clinical observations that are reported in [22]. The mean-average (the temporal mean over the cardiac cycle and the spatial average along the wall) wall shear stress is shown in Figure 9. An interesting result is that the wall shear stress does not increase linearly with the degree of stenosis. It increases sharply at around 70% occlusion. The *in vivo* study by Merino *et al.* [72] showed that although platelets formed a mural thrombus in all the vascular injury models, which ranged from 0 to 92% stenosis, the thrombus progressed to occlusion only if the stenosis severity was greater than 60%. Our results suggest a similar phenomenon where an occlusion of more than 70% of the artery may result in dangerous medical condition for its rapid increase in the wall shear stress. Regions of low and oscillating wall shear stress persist in the downstream regions of the constriction as the degree of the stenosis increases as shown in Figure 10. For mild (40%) stenosis, the oscillations are quickly washed out and the low (negative) wall shear stress region is concentrated in the vicinity of the root of the constriction. As the stenosis grows, oscillations and low shear regions develop further downstream.

4.2.3. Residence time. As the degree of stenosis increases, up to 76%, the location of maximum residence time is located farther and farther from the constriction as shown in Figure 10. The magnitude of residence time increases for up to 60% stenosed arteries. Then, for higher degrees of stenosis, the residence time decreases and reaches a very low value at 76%. This result shows that the particle residence time does not correlate proportionally with the degree of stenosis. For high degrees of stenosis, platelets tend to be washed out faster by rapidly changing flow and particle residence time is shorter. It is safe to conclude that the growth of intima will not be exacerbated by the particle residence time after the lesion is formed because the particle residence time appears to reduce at high degrees of stenosis.

DOI: 10.1002/fld

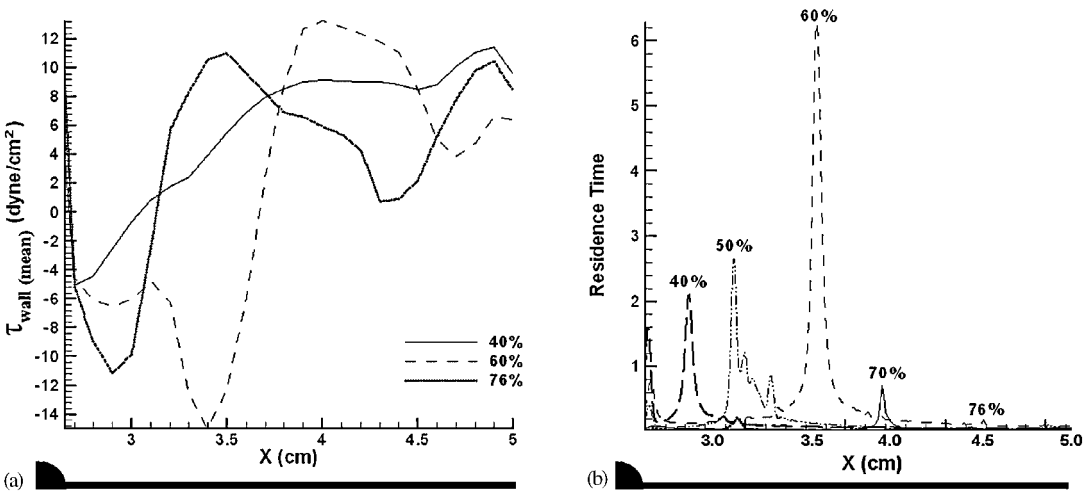

Figure 10. Mean wall shear stress and residence time downstream of the constriction for varying degrees of stenosis: (a) mean wall shear stress and (b) residence time.

5. STENTED ARTERY

We now consider the flow in a vessel where an interventional device such as a stent is inserted. A stent, a wire frame used to support the artery, is very effective in opening up the lumen in a stenosed vessel. The study of blood flow dynamics is very complex around the wall where the stent in deployed because many mechanical and geometric characteristics are involved. Thus, it is necessary to simplify the model while maintaining reasonable physiologic conditions. We first assume that the artery has a constant length and diameter. The model geometry includes only the wire structure and the vessel wall. No consideration is given to the appearance of thrombus that can occur within minutes to hours after stent implantation. The stent strut is $\lambda_s = 0.008\,\text{cm}$ in thickness and $t_s = 0.008\,\text{cm}$ wide. Each strut is separated by 0.03 cm from each other. The stent considered in this model is $L_s = 0.8\,\text{cm}$ long with 22 identical struts and implanted at $X = 2.0\,\text{cm}$ from the entrance of the artery as shown in Figure 11. The fluid model, boundary, and initial conditions and properties are the same as the ones detailed in the previous flow in carotid artery examples.

5.1. Velocity

A velocity vector plot between two adjacent stent struts (near the eighth stent strut) at different periods of the cardiac cycle is shown in Figure 12. Large fluid perturbations start to appear at the tip of the strut. A clockwise vortex with a low magnitude forms at the beginning of diastole ($t = 2.05\,\text{s}$) and disappears at the end of diastole ($t = 2.20\,\text{s}$). This slow moving vortex is destroyed rapidly by reversing flows. The velocity of this vortex is very small compared with the velocity observed above the stent wires. For instance, at the end of systole, the velocity in the mainstream (centerline of the artery) is approximately 41.6 cm/s. However, the maximum velocity within the recirculation zone is 1.49 cm/s or about 3.5% of the maximum velocity. This is in agreement with previous results [46, 73]. Thus, these flow patterns should not be viewed as strong vortices, but rather as zones of stagnation.

DOI: 10.1002/fld

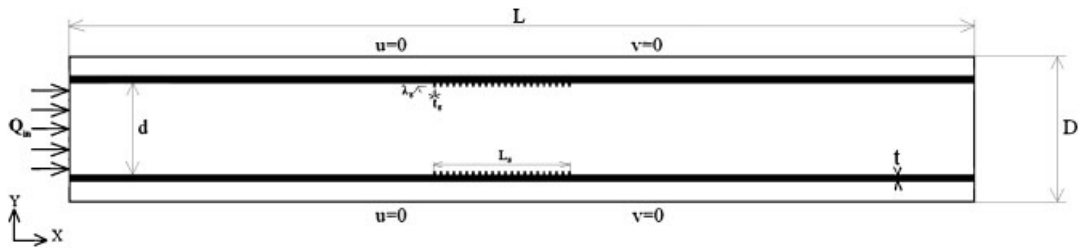

Figure 11. Pulsatile flow in a stented carotid artery.

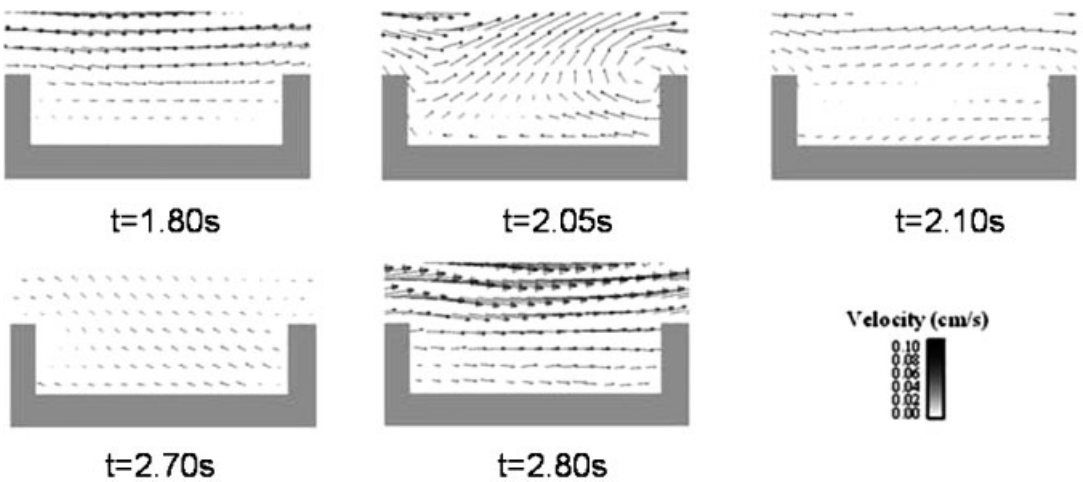

Figure 12. Velocity vector plot inside a stented region during a cardiac cycle.

5.2. *Shear stress*

We now quantify the wall shear stress between the stent branches. For the most part of the unstented region, the mean-average wall shear stress value is 8.47 dyn/cm^2, which agrees with our previous result in Section 3. In the stented region, we observed a significant decrease along the inner strut wall in the mean and peak space-dependent wall shear stress distribution shown in Figure 13. A low mean shear stress zone ($<$5.0 dyn/cm^2) is observed in between stent struts. A mean-average value of 5.32 dyn/cm^2 is found in between the stent struts. Higher shear stress values are found on or near the stent struts where the maximum mean shear stress measured in this region is 18.01 dyn/cm^2. The peak wall shear stress measured at the end of systole ranges between 13 and 108 dyn/cm^2. Our numerical results compared quite well with those reported by Benard *et al.* [45], which had 15 dyn/cm^2 for shear stress measured near a stent strut, and Wentzel *et al.* [43] who found wall shear stress from simulations varying from 3 to 90 dyn/cm^2.

In most stents, the site with the greatest stress concentration is at the entrance of the stent. This is particularly apparent in our model as shown in Figure 14 where high or low wall shear stress

DOI: 10.1002/fld

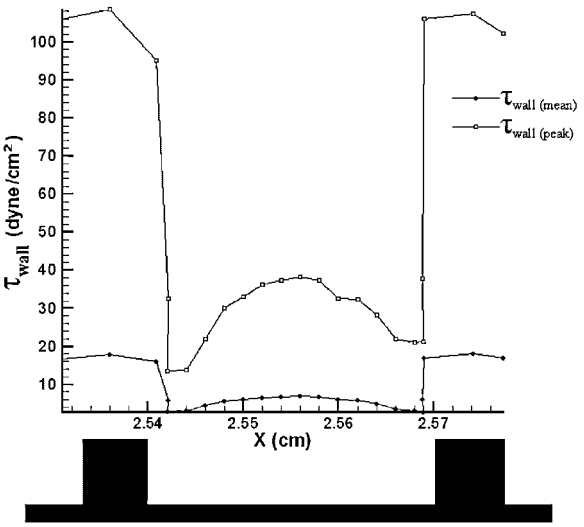

Figure 13. Mean and peak wall shear stresses inside one central strut of the stent.

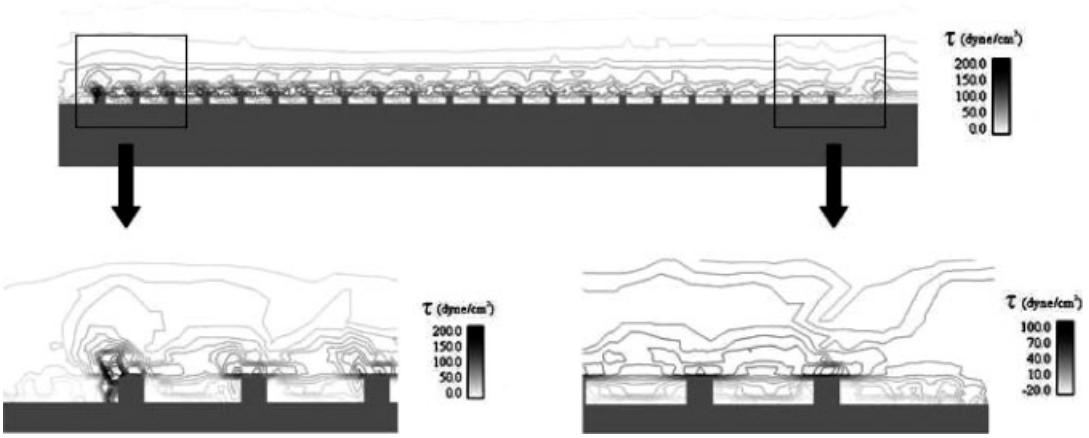

Figure 14. Shear stress contours along the stent and artery wall with zoomed entrance and exit of the stented region.

is observed at the ends of the stent. In the central part of the stented area, the pattern detailed previously appears repetitively. The fluid–structure interaction between the stent wire and the blood flow alters the wall shear stress at the entrance and the exit. At the entrance, it shows a remarkably high wall shear stress concentration of 212.5 dyn/cm^2. At the exit, a large low and oscillating wall shear stress area forms behind the stented region.

DOI: 10.1002/fld

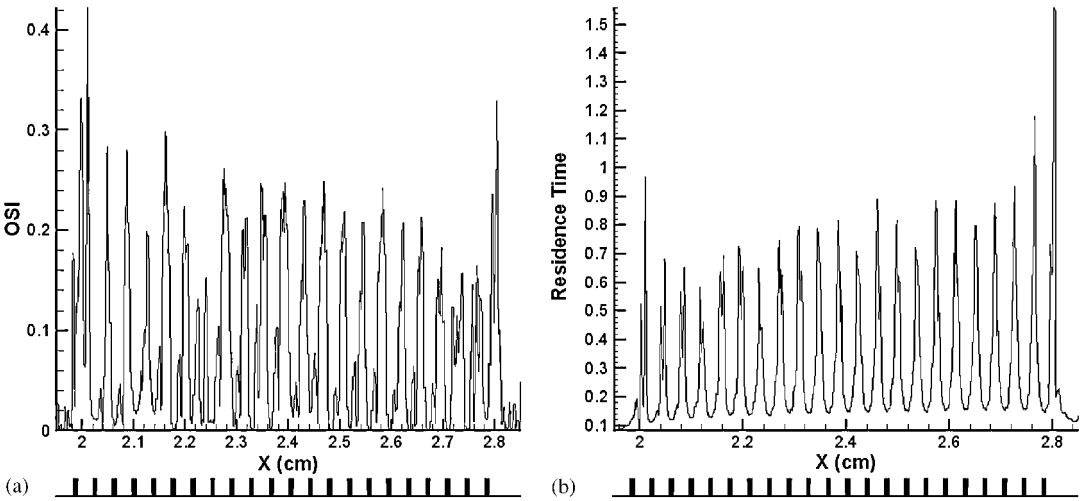

Figure 15. Oscillatory shear index and residence time along the stented region: (a) oscillatory shear index and (b) residence time.

5.3. Oscillatory shear index

The OSI distribution along the stented region is presented in Figure 15 to characterize the transient nature of arterial flow fields. The corresponding stent is drawn at the bottom of the figure to identify the regions with minimum and maximum values. For struts located in the middle of the stent, OSI sharply increases to an average value of 0.23 in between struts. At both ends, the OSI reaches maximum values of 0.42 at the entrance and 0.33 at the exit of the stented region. This means that the wall is subjected to high oscillatory shear stresses at both ends, while at the center of the stented region the oscillatory behavior of the wall shear stress is diminished. From the analysis of the OSI, we can conclude that the flow reversal between each strut depicted in Figure 12 is more important at the entrance and around the last strut of the stented region.

5.4. Residence time

The characteristic residence time along the stented region is evaluated as shown in Figure 15(b). The residence time is much higher at the entrance (first strut) and the exit of the stent. A particle is twice more likely to be trapped in a strut at the entrance and/or at the exit of the stented region than at any other centered strut of the stent.

According to our results, it is likely that the platelets are activated at the entrance of the stent due to high wall shear stress and high OSI. We then observe repetitive patterns for velocity and wall shear stress along the stented region, characterized by flow recirculation and low wall shear stress. Since most intimal thickening occurs where the average wall shear stress is less than $5.0\,\mathrm{dyn/cm^2}$, the whole stented region presents restenosis risk for all surfaces close to stent wire. The exit, which has a high residence time, may be a favorable spot for adhesion and accumulation of platelets. This higher blood residence time increases the exposure time of blood elements and provides an environment prone to thrombosis. The *in vitro* studies of Sprague *et al.* [74], with cell growth in stagnation zone and along the stent strut, corroborate our numerical results.

DOI: 10.1002/fld

6. CONCLUSIONS

Blood flow in idealized physiologic vascular models of healthy, stenosed, and stented carotid arteries was simulated and studied quantitatively. The hemodynamic quantities such as the velocity profiles, shear stress, OSI, and particle residence time were analyzed for stenosed and stented arteries using the IFEM. A healthy artery was first studied to establish a baseline comparison. The diseased and stented arteries are found to have significantly higher and oscillating wall shear stresses than a healthy artery. In a stenosed artery, we found a high wall shear stress at the stenosed throat, a low and oscillating wall shear stress downstream of the stenosis, and a high residence time immediately downstream of the stenosis. In the stented artery, the wall shear stress and the residence time are the highest at the entrance and the exit of the stent, while they decrease significantly in between stent struts. The results suggested that platelets/particles are most likely to be activated near the entrance; they form aggregates in between struts where the shear stress is very low and eventually reside at the end of the stent where the residence time is the highest. The simulations and analysis presented in this paper will be helpful for defining biomarkers and obtaining optimal stent designs, which can potentially minimize hemodynamic effects prone to thrombosis. Optimizing the shape and geometry of these types of medical devices to minimize unfavorable fluid mechanical effects will contribute to the prevention and intervention of serious cardiovascular diseases.

REFERENCES

1. American Heart Association. *Heart Disease and Stroke Statistics*. American Heart Association: Dallas, TX, 2002.
2. Bogousslavski J, Van Melle G, Regli F. The Lausanne stroke registry: analysis of 1000 consecutive patients with first stroke. *Stroke* 1988; **19**:1083–1092.
3. Mohr JP, Caplan LR, Melski JW, Goldstein RJ, Duncan GW, Kistler JP, Pessin MS, Bleich HL. The Harvard cooperative stroke registry: a prospective registry. *Neurology* 1978; **28**:754–762.
4. Golledge J, Greenhalgh RM, Davies AH. The symptomatic carotid plaque. *Stroke* 2000; **31**(3):774–781.
5. Canic S, Mikelic A, Tambaca J. A two-dimensional effective model describing fluid–structure interaction in blood flow: analysis, simulation and experimental validation. *Special Issue of Comptes Rendus Mechanique* 2005; **333**(12):867–883.
6. Giddens DP, Zarins CK, Glagov S. Response of arteries to near-wall fluid dynamic behavior. *Applied Mechanics Reviews* 1990; **43**:98–102.
7. Mittal R, Simmons SP, Najjar F. Numerical study of pulsatile flow in a constricted channel. *Journal of Fluid Mechanics* 2003; **485**:337–378.
8. Perktold K, Resch M, Peter RO. Three-dimensional numerical analysis of pulsatile flow and wall shear stress in the carotid artery bifurcation. *Journal of Biomechanics* 1991; **24**(6):409–420.
9. Siegel JM, Markou CP, Ku DN, Hanson SR. A scaling law for wall shear stress through an arterial stenosis. *Journal of Biomechanical Engineering* 1994; **116**:446–451.
10. Taylor CA, Hughes TJR, Zarins CK. Finite element modeling of blood flow in arteries. *Computer Methods in Applied Mechanics and Engineering* 1998; **158**:155–196.
11. Malek AM, Alper SL, Izumo S. Hemodynamic shear stress and its role in atherosclerosis. *Journal of the American Medical Association* 1999; **282**:2035–2042.
12. Bluestein D *et al.* Steady flow in an aneurysm model: correlation between fluid dynamics and blood platelet deposition. *Journal of Biomechanical Engineering* 1996; **118**(3):280–286.
13. Bluestein D *et al.* Fluid mechanics of arterial stenosis: relationship to the development of mural thrombus. *Annals of Biomedical Engineering* 1997; **25**(2):344–356.
14. Folts JD, Crowell EB, Rowe GG. Platelet aggregation in partially obstructed vessels and its elimination with aspirin. *Circulation* 1976; **54**:365–370.
15. Reese JM, Thompson DS. Shear stress in arterial stenoses: a momentum integral model. *Journal of Biomechanics* 1998; **31**(11):1051–1057.

DOI: 10.1002/fld

16. Tu C, Deville M, Dheur L, Vanderschuren L. Finite element simulation of pulsatile flow through arterial stenosis. *Journal of Biomechanics* 1992; **25**(10):1142–1152.
17. Ku DN, Giddens DP, Zarins CK, Glagov S. Pulsatile flow and atherosclerosis in the human carotid bifurcation. Positive correlation between plaque location and low oscillating shear stress. *Arteriosclerosis* 1985; **5**:293–302.
18. Wootton DM, Ku DN. Fluid mechanics of vascular systems, diseases, and thrombosis. *Annual Review of Biomedical Engineering* 1999; **1**:299–329.
19. Friedman MH, Hutchins GM, Bargeron CB, Deters OJ, Mark FF. Correlation of human arterial morphology with hemodynamic measurements in arterial casts. *Journal of Biomechanical Engineering* 1981; **103**:204–207.
20. He X, Ku DN. Pulsatile flow in the human left coronary artery bifurcation: average conditions. *Journal of Biomechanical Engineering* 1996; **118**:74–82.
21. Moore JE, Guggenheim N, Delfino A, Doriot PA, Dorsaz PA, Rutishauser W, Meister JJ. Preliminary analysis of the effects of blood vessel movement on blood flow patterns in the coronary arteries. *Journal of Biomechanical Engineering* 1994; **116**:302–306.
22. Giddens DP, Zarins CK, Glagov S. The role of fluid mechanics in localization and detection of atherosclerosis. *Journal of Biomechanical Engineering* 1993; **115**:588–594.
23. Glagov S. Intimal hyperplasia, vascular modeling, and the restenosis problem. *Circulation* 1994; **89**:2888–2891.
24. Lee D, Chiua YL, Jen CJ. Platelet adhesion onto the wall of a flow chamber with an obstacle. *Biorheology* 1997; **34**(2):111–126.
25. Zarins CK. Hemodynamic factors in atherosclerosis. In *Vascular Surgery*: *A Comprehensive Review*, Moore W (ed.). W.B. Saunders Co.: Philadelphia, 1993.
26. Lei M, Kleinstreuer C, Truskey GA. Numerical investigation and prediction of atherogenic sites in branching arteries. *Journal of Biomechanical Engineering* 1995; **117**:350–357.
27. Tang D, Yang C, Huang Y, Ku DN. Wall stress and strain analysis using a 3-d thick-wall model with fluid–structure interactions for blood flow in carotid arteries with stenoses. *Computers and Structures* 1999; **72**:341–356.
28. Tang D, Yang J, Yang C, Ku DN. A nonlinear axisymmetric model with fluid–wall interactions for viscous flows in stenotic elastic tubes. *Journal of Biomechanical Engineering* 1999; **121**:494–501.
29. Tang D, Yang C, Huan D, Ku DN. Effects of stenosis asymmetry on blood flow in stenotic arteries and wall compression. *Advances in Bioengineering* 1999; **43**:75–76.
30. Liu B, Tang D. A finite element solution of viscous flow in collapsible tubes with stenosis. *Applied Numerical Mathematics* 2000; **32**:87–101.
31. Tang D, Yang J. A free moving boundary model and boundary iteration method for unsteady viscous flow in stenotic elastic tubes. *SIAM Journal on Scientific Computing* 2000; **21**:1370–1386.
32. Tang D, Chen XK, Yang C, Kobayashi S, Ku DN. Effects of dynamic wall properties on blood flow in stenotic arteries. *Journal of Medical Biomechanics* 2000; **15**:77.
33. Friedrich P, Reininger AJ. Occlusive thrombus formation on indwelling catheters: in vitro investigation and computational analysis. *Thrombosis and Haemostasis* 1995; **73**(1):66–72.
34. Moake JL, Turner NA, Stathopoulos NA, Nolasco LH, Hellums JD. Shear-induced platelet aggregation can be mediated by vwf released from platelets, as well as by exogenous large or unusually large vwf multimers, requires adenosine diphosphate, and is resistant to aspirin. *Blood* 1988; **71**:1366–1374.
35. Reininger AJ, Heinzmann U, Reininger CB, Friedrich P, Wurzinger LJ. Flow mediated fibrin thrombus formation in an endothelium-lined model of arterial branching. *Thrombosis Research* 1994; **74**(6):629–641.
36. Barstad RM, Kierulf P, Sakariassen KS. Collagen induced thrombus formation at the apex of eccentric stenosis: a time course study with non-anticoagulated human blood. *Thrombosis and Haemostasis* 1996; **75**(4):685–692.
37. Brown BG, Gallery CA, Badger RS, Kennedy JW, Mathey D, Bolson EL, Dodge HT. Incomplete lysis of thrombus in the moderate underlying atherosclerotic lesion during intracoronary infusion of streptokinase for acute myocardial infarction: quantitative angiographic observations. *Circulation* 1986; **73**(4):653–661.
38. Falk E. Coronary thrombosis: pathogenesis and clinical manifestations. *American Journal of Cardiology* 1991; **68**(7):28–35.
39. Reininger AJ, Reininger CB, Heinzmann U, Wurzinger LJ. Residence time in niches of stagnant flow determines fibrin clot formation in an arterial branching model: detailed flow analysis and experimental results. *Thrombosis and Haemostasis* 1995; **74**(3):916–922.
40. Holmes DR, Hirshfeld J, Faxon D, Vlietstra RE, Jacobs A, King SB, Bashore TM, Bridges ND, Higgins CB, Hiratzka LF, Little WC, Magorien RD, Nocero MA, Oesterle S, Vogel RA, Forrester JS, Douglas PS, Faxon DP, Fisher JD, Gibbons RJ, Halperin JL, Hutter AM, Hochman JS, Kaul S, Weintraub WS, Winters WL, Wolk MJ. Coronary artery stents. *Journal of the American College of Cardiology* 1998; **32**:1471–1482.

DOI: 10.1002/fld

41. Ikari Y, Hara K, Tamura T, Saeki F, Yamaguchi T. Luminal loss and site of restenosis after Palmaz–Schatz coronary stent implantation. *American Journal of Cardiology* 1995; **76**:117–120.
42. Wentzel JJ, Krams R, Schuurbiers JCH, Oomen JA, Kloet J, van der Giessen WJ, Serruys PW, Slager CJ. Relationship between neointimal thickness and shear stress after wallstent implantation in human coronary arteries. *Circulation* 2001; **103**:1740–1745.
43. Wentzel JJ, Whelan DM, van der Giessen WJ, van Beusekom HMM, Andhyiswara I, Serruys PW, Slager CJ, Krams R. Coronary stent implantation changes 3-d vessel geometry and 3-d shear stress distribution. *Journal of Biomechanics* 2000; **33**:1287–1295.
44. Natarajan S, Mokhtarzadeh-Dehghan MR. A numerical and experimental study of periodic flow in a model of a corrugated vessel with application to stented arteries. *Medical Engineering and Physics* 2000; **22**:555–566.
45. Benard N, Coisne D, Donal E, Perrault R. Experimental study of laminar blood flow through an artery treated by a stent implantation: characterization of intra-stent wall shear stress. *Journal of Biomechanics* 2003; **36**:991–998.
46. Berry JL, Santamarina A, Moore Jr JE, Roychowdhury S, Routh WD. Experimental and computational flow evaluation of coronary stents. *Annals of Biomedical Engineering* 2000; **28**:386–398.
47. Zhang LT, Gay M. Immersed finite element method for fluid–structure interactions. *Journal of Fluids and Structures* 2007; **23**(6):839–857.
48. Zhang LT, Gerstenberger A, Wang X, Liu WK. Immersed finite element method. *Computer Methods in Applied Mechanics and Engineering* 2004; **193**:2051–2067.
49. Liu Y, Zhang LT, Wang X, Liu WK. Coupling of Navier–Stokes equations with protein molecular dynamics and its application to hemodynamics. *International Journal for Numerical Methods in Fluids* 2004; **46**(12):1237–1252.
50. Gay M, Zhang LT, Liu WK. Stent modeling using immersed finite element method. *Computer Methods in Applied Mechanics and Engineering* 2006; **195**:4358–4370.
51. Zhang LT, Gay M. Characterizing left atrial appendage functions in sinus rhythm and atrial fibrillation using computational models. *Journal of Biomechanics* 2008; **41**:2515–2523.
52. Zhang LT, Gay M. Imposing rigidity constraints on immersed objects in unsteady fluid flow. *Computational Mechanics* 2008; **42**:357–370.
53. Li S, Liu WK. Meshfree and particle methods and their applications. *Applied Mechanics Review* 2002; **55**:1–34.
54. Liu WK, Jun S, Zhang YF. Reproducing kernel particle methods. *International Journal for Numerical Methods in Fluids* 1995; **20**:1081–1106.
55. Himburg HA, Grzybowski DM, Hazel AL, LaMack JA, Li XM, Friedman MH. Spatial comparison between wall shear stress measures and porcine arterial endothelial permeability. *American Journal of Physiology—Heart and Circulatory Physiology* 1922; **286**:1916–1922.
56. Holdsworth DW, Norley CJD, Frayne R, Steinman DA, Rutt BK. Characterization of common carotid artery blood-flow waveforms in normal human subjects. *Physiological Measurement* 1999; **20**:219–240.
57. Caro CG, Pedley TJ, Schroter RC, Seed WA. *Mechanics of the Circulation*. Oxford University Press: Oxford, 1978.
58. Berbich L, Bensalah A, Flaud P, Benkirane R. Non-linear analysis of the arterial pulsatile flow: assessment of a model allowing a non-invasive ultrasonic functional exploration. *Medical Engineering and Physics* 2001; **23**:175–183.
59. Dammers R, Stifft F, Tordoir JHM, Hameleers JMM, Hoeks APG, Kitslaar PJEHM. Shear stress depends on vascular territory: comparison between common carotid and brachial artery. *Journal of Applied Physiology* 2003; **94**:485–489.
60. Gnasso A, Carallo C, Irace C, Spagnuolo V, De Novara G, Mattioli PL, Pujia A. Association between intima-media thickness and wall shear stress in common carotid arteries in healthy male subjects. *Circulation* 1996; **94**:3257–3262.
61. Gnasso A, Carallo C, Irace C, De Franceschi MS, Motti C, Mattioli PL, Pujia A. In vivo association between low wall shear stress and plaque in subjects with asymmetrical carotid atherosclerosis. *Stroke* 1997; **28**:993–998.
62. Hoeks APG, Samijo SK, Brands PJ, Reneman RS. Noninvasive determination of shear-rate distribution across the arterial lumen. *Hypertension* 1995; **26**:26–33.
63. Oshinski JN, Curtin JL, Loth F. Mean-average wall shear stress measurements in the common carotid artery. *Journal of Cardiovascular Magnetic Resonance* 2006; **8**:1–6.
64. Oyre S, Ringgaard S, Kozerke S *et al.* Accurate noninvasive quantitation of blood flow, cross-sectional lumen vessel area and wall shear stress by three-dimensional paraboloid modeling of magnetic resonance imaging velocity data. *Journal of the American College of Cardiology* 1998; **32**:128–134.

DOI: 10.1002/fld

65. Samijo SK, Willigers JM, Brands PJ, Barkhuysen R, Reneman RS, Kitslaar PJEHM, Hoeks APG. Reproducibility of shear rate and shear stress assessment by means of ultrasound in the common carotid artery of young human males and females. *Ultrasound in Medicine and Biology* 1997; **23**(4):583–590.
66. Rosenfeld M, Einav S. The effect of constriction size on the pulsatile flow in a channel. *Journal of Fluids Engineering* 1995; **117**:571–576.
67. Zhang JN, Bergeron AL, Yu Q, Sun C, McBride L, Bray PF. Duration of exposure to high shear stress is critical in shear-induced platelet activation–aggregation. *Thrombosis and Haemostasis* 2003; **90**:672–678.
68. Holme PA, Orvim U, Hamer MJAG, Solum NO, Brosstad FR, Barstad RM, Sakariassen KS. Shear-induced platelet activation and platelet microparticle formation at blood flow conditions as in arteries with a severe stenosis. *Arteriosclerosis Thrombosis and Vascular Biology* 1997; **17**(4):646–653.
69. Sakariassen KS, Holme PA, Orvim U, Barstad RM, Solum NO, Brosstad FR. Shear-induced platelet activation and platelet microparticle formation in native human blood. *Thrombosis Research* 1998; **92**(6):33–41.
70. Longest PW, Kleinstreuer C. Comparison of blood particle deposition models for non-parallel flow domains. *Journal of Biomechanics* 2003; **36**:421–430.
71. Kunov MJ, Steinman DA, Ethier CR. Particle volumetric residence time calculations in arterial geometries. *Journal of Biomedical Engineering* 1996; **118**:158–164.
72. Merino A, Cohen M, Badimon JJ, Fuster V, Badimon L. Synergistic action of severe wall injury and shear forces on thrombus formation in arterial stenosis: definition of a thrombotic shear rate threshold. *Journal of the American College of Cardiology* 1994; **24**(4):1091–1097.
73. Ladisa Jr JF, Hettrick DA, Olson LE, Guler I, Gross ER, Kress TT, Kersten JR, Warltier DC, Pagel PS. Stent implantation alters coronary artery hemodynamics and wall shear stress during maximal vasodilation. *Journal of Applied Physiology* 2002; **93**:1939–1946.
74. Sprague EA, Luo J, Palmaz JC. Human aortic endothelial cell migration onto stent surfaces under static and flow condition. *Journal of Vascular and Interventional Radiology* 1997; **8**:83–92.

DOI: 10.1002/fld